Supporting Information

Femtosecond Charge Density Modulation in Photoexcited $CuWO_4$

Yohei Uemura,[a,b,$#] Ahmed S. M. Ismail,[a#] Sang Han Park,[c] Soonnam Kwon,[c] Minseok Kim,[c] Yasuhiro Niwa,[d] Hiroki Wadati,[e,f] Hebatalla Elnaggar,[a] Federica Frati,[a] Ties Haarman,[a] Niko Höppel,[j] Nils Huse,[j] Yasuyuki Hirata,[e] Yujun Zhang,[e,$$] Kohei Yamagami,[e] Susumu Yamamoto,[e] Iwao Matsuda,[e] Tetsuo Katayama,[g,h] Tadashi Togashi,[g,h] Shigeki Owada,[g,h] Makina Yabashi,[h] Uufuk Halisdemir,[i] Gertjan Koster,[i] Toshihiko Yokoyama[k], Bert M. Weckhuysen,[a] and Frank M. F. de Groot[a*]

a. Inorganic Chemistry and Catalysis, Debye Institute for Nanomaterials Science, Utrecht University, Universiteitslaan 99, 3584 CG Utrecht, The Netherlands

b. Institute for Catalysis, Hokkaido University, Kita 21 Nishi 10, Kita-ku, Sapporo, Hokkaido 001-0021, Japan

c. PAL-XFEL, Pohang Accelerator Laboratory, 77 Cheongam-Ro, Nam-Gu, Pohang, Gyeongbuk 37673, South Korea

d. Photon Factory, Institute for Materials Structure Science, KEK, Tsukuba 305-0801, Japan

e. Institute for Solid State Physics, University of Tokyo, Kashiwa, Chiba 277-8581, Japan

f. Graduate School of Material Science, University of Hyogo, Kamigori, Hyogo 678-1297, Japan

g. JASRI, Kouto, Sayo-cho, Hyogo 679-5198, Japan

h. RIKEN SPring-8 Center, Kouto Sayo-cho, Hyogo 679-5148, Japan

i. Faculty of Science and Technology and MESA+ Institute for Nanotechnology, University of Twente, P.O. Box 2171, 7500 AE Enschede, The Netherlands

j. Department of Physics and Center for Free-Electron Laser Science, University of Hamburg, Luruper Chaussee 149, 22761 Hamburg, Germany

k. Institute for Molecular Science, Myodaiji-cho, Okazaki 444-8585, Japan

[$]the current address: Laboratory for Environmental Chemistry (LUC), Energy and Environmental Research Division (ENE), Paul Scherrer Institute

PSI, Forschungsstrasse 111, 5232 Villigen, Switzerland

[$$]the current address: Institute of High Energy Physics, Chinese Academy of Sciences Yuquan Road 19B, Shijingshan District, Beijing, 100049, China

E-mail: f.m.f.degroot@uu.nl

#These authors contributed equally to this work.

1) Copper Tungstate Thin Film Fabrication and Characterization

A 50 nm copper tungstate ($CuWO_4$) thin film was deposited on indium tin oxide (ITO)/fused silicon dioxide substrate by pulsed laser deposition at the University of Twente, The Netherlands. First, a 5 nm ITO thin film was deposited on a fused silicon dioxide substrate by translating a KrF excimer laser (λ = 248 nm) on a rotating ITO target with an incident angle of 45° with a fluency of 2 J cm^{-2} and a repetition rate of 1 Hz. The ITO target was then replaced with $CuWO_4$ target and $CuWO_4$ thin-film was deposited at the same deposition conditions. The deposition experiment was conducted at 700 °C and under 1.3 kPa oxygen pressure.

The thin film surface morphology was studied with scanning electron microscopy (SEM) using FEI Helios Nanolab G3 at 5 kV acceleration voltage (cf. Figure S1a). Different spots in the samples were investigated to ensure the surface homogeneity. To confirm the formation of the $CuWO_4$ triclinic phase, X-ray Diffraction (XRD) using a Bruker D2 Phaser diffractometer with Co $K\alpha_{1,2}$ radiation (λ = 1.789 Å). XRD measurements were conducted between $10° < 2\theta < 90°$ every 0.14° with 3 $s \cdot step^{-1}$. Background subtraction was conducted by DiffracEvaluation software, and the data was plotted in Origin. Comparing to the previous results[1], the characteristic diffraction patters of $CuWO_4$ was observed by the XRD measurements (the peaks of $CuWO_4$ are denoted by triangles in Figure S1 (b).) We hence conclude that a $CuWO_4$ thin film was successfully formed on the fluorine-doped tin oxide (FTO) substrate.

Hard X-ray Photoelectron Spectroscopy (HAXPES) scan was recorded in the HIKE station (beamline KMC-1) at BESSY II synchrotron, where the spectral features of both elements at different kinetic energies (different depths in the sample) confirm the presence of Cu^{2+} (Figure S1d) and W^{6+} in $CuWO_4$ (Figure S1c).

The surface morphology of the $CuWO_4$ thin film was observed by Atomic Force Microscopy (AFM) displayed in Figure S1 (e). From the AFM image, the thin film was formed homogeneously on the FTO

substrate and the average surface roughness of the $CuWO_4$ thin film was determined to be ~5 nm. Considering the penetration depth of fluorescence X-ray at the Cu L_3 edge, the roughness of the sample surface would not affect the XAS measurements. A UV-Vis spectrum of the prepared $CuWO_4$ is shown in Figure S1 (f) and the bandgap was estimated to be ~2.3 eV.

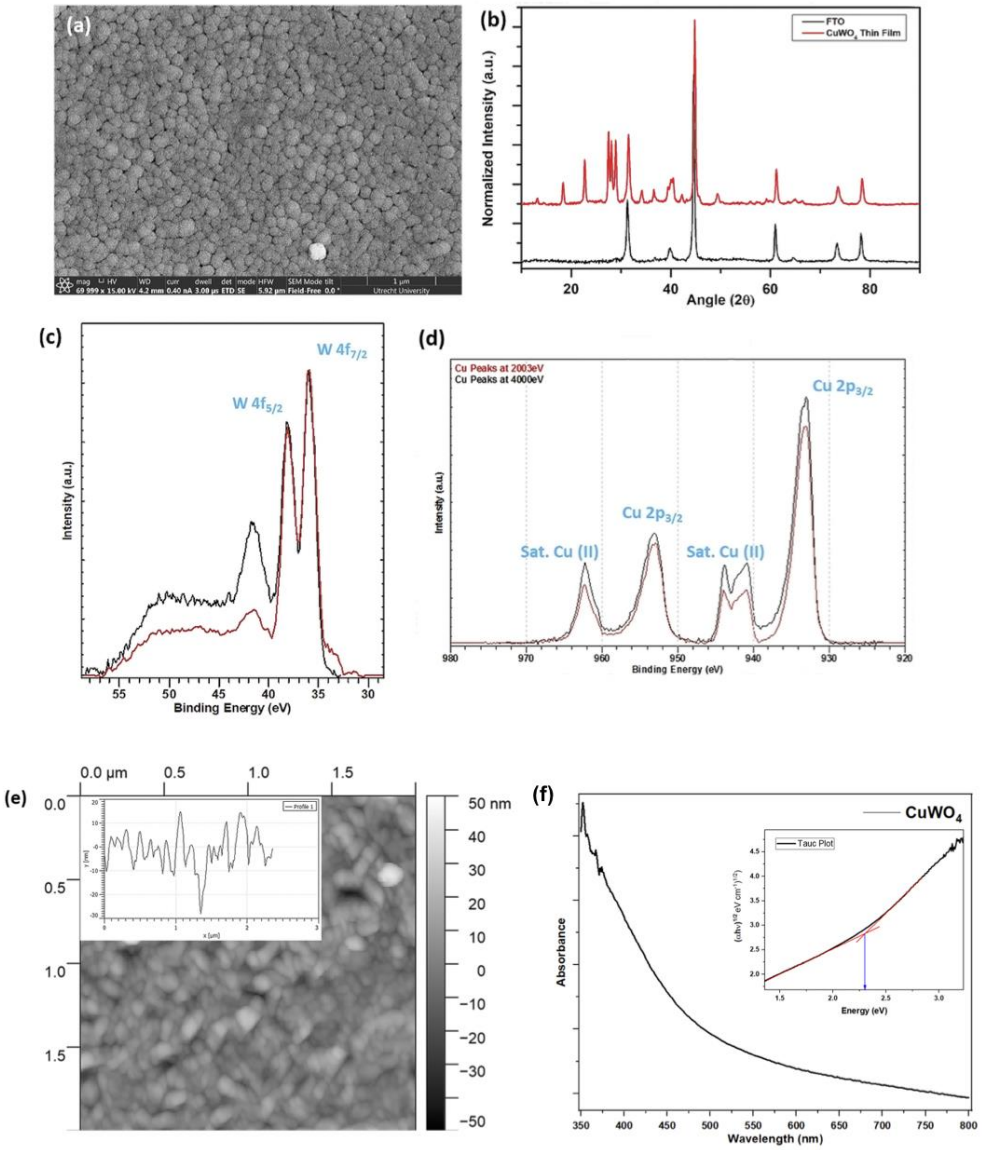

Figure S1. Physical and chemical characterization of the $CuWO_4$ thin films. (a) Scanning electron microscopy (SEM) image, (b) X-ray diffraction (XRD) of $CuWO_4$ and the underlying fluorine-doped tin oxide (FTO) layer, (c) W 4f and (d) Cu 2p X-ray photoelectron spectroscopy (XPS) at different kinetic energies, and (e) atomic force microscopy (AFM) image of the $CuWO_4$ thin film. (f) A UV-Vis spectrum of the $CuWO_4$ thin film and Tauc plot of it (inset). In Figure S1 (B), the characteristic X-ray diffraction features of $CuWO_4$ are denoted by triangles. [1]

2) Time-resolved Optical Spectroscopy on $CuWO_4$

Time-resolved UV-Vis measurements were conducted on a 15nm $CuWO_4$ thin film that was deposited on a 100 nm silicon nitride substrate by pulsed laser deposition. A 3 kHz Ti:sapphire amplified laser system (Spectra Physics Spitfire Ace, 90 fs, 800 nm) was employed to investigate the sample. Frequency-doubled 400-nm pulses excited the sample with a flux of 4.6 mJ/cm² and a super-continuum pulse (generated in a 1-mm sapphire plate) probed the absorbance change in transmission using a prism-based imaging spectrograph and a CCD detector. A second super-continuum pulse served as a reference pulse and was detected in the same imaging spectrograph with a second CCD detector. Slight spatial spill-over of probe and reference beam on the detector arrays cause the spectral interference at wavelength longer than 600 nm. The data was chirp-corrected in silico by using the delay at half rise of the signal onset for every wavelength. The substrate did not generate a measurable cross phase modulation signal that could have provided a direct measure of super-continuum chirp.

The results of transient optical pump probe spectroscopy of $CuWO_4$ are displayed in Figure S2. After the photoexcitation, a broad transient absorption is observed with a maximum around 620 nm (panel B). Since this is the first report about the femtosecond transient optical spectroscopy of $CuWO_4$ to the best of our knowledge, there is no literature to propose the assignments of the transient absorption. Considering the previous transient optical spectroscopic studies on WO_3 [2, 3], the absorbance above 600 nm may be assigned to the electrons in the conduction band. The absorption from the holes in the valence band is supposed to be observed below 500 nm. A tendency of increased transient absorption below 420 nm wavelength is superposed with scatter from the 400-nm excitation pulses. The experiment was not setup to probe transient absorption below 420 nm. Therefore, we did not obtain result that may be attributed exclusively to hole absorption.

The kinetic traces at the four wavelengths 475 nm, 526 nm, 574 nm, and 626 nm are displayed in panel C of Figure S2. The transient absorption spectra were measured up to 1 ns with only residual absorbance changes of less than 0.5 mOD observable at the longest delay. We found that the response can be fully and globally modeled with a simplified sequential rate-equation model consisting of four excited states:

$$\Delta A(\lambda) = \frac{1}{2}\left\{\mathrm{erf}\left(\frac{t-t_0}{\sqrt{2}\sigma} - \frac{\sigma}{\sqrt{2}\tau_1}\right)+1\right\}\left[a_1(\lambda)\cdot e^{-\frac{t-t_0}{\tau_1}+\frac{\sigma^2}{2\tau_1^2}} + a_2(\lambda)\cdot\left(e^{-\frac{t-t_0}{\tau_2}} - e^{-\frac{t-t_0}{\tau_1}+\frac{\sigma^2}{2\tau_1^2}}\right)\ldots + a_3(\lambda)\right.$$
$$\left.\cdot\left(e^{-\frac{t-t_0}{\tau_3}} - e^{-\frac{t-t_0}{\tau_2}}\right) + a_4(\lambda)\cdot\left(e^{-\frac{t-t_0}{\tau_4}} - e^{-\frac{t-t_0}{\tau_3}}\right)\right] + \Delta A_0.$$

The model assumes a Gaussian response function with σ = (45±1) fs. Because τ_1 only similarly short to σ, we have only included the proper convolution factors for τ_1 into the model. Four distinct time-constants, τ_1 = (140±5) fs, τ_2 = (1.5±0.2) ps, τ_3 = (27±5) ps, and τ_4 = (733±63) ps, can be identified in a global fit to the four kinetic time traces in panel C which suggests that the observed absorbance changes in the visible are attributable to one response rather than several response processes.

The time-constants $\tau_{i=1,2,3,4}$ sort into separate orders of magnitude which also justifies not using the analytic solution of a rate-equation model with four excited states which decay sequentially (1→2→3→4→0). We could have attempted to further simplify the model to a sum of four exponential decays for which we would expect very similar results but we opted for the above model for a clear separation of responses in time. Note that the uncertainties of the above time-constants derive from the Hessian of the Levenberg-Marquardt fit algorithm. These numbers do not represent the experimental error as they are model and constraint dependent. The first time-constant is very robust because the associated fast dynamics dominate the induced absorption change which has decayed to about one third of its peak value by 500 fs. In principle, we can also force a time constant τ_2' = 400 fs and find an acceptable fit with τ_1' = (136±9) fs, τ_3' = (4.8±0.5) ps, and τ_4' = (544±29) ps. The largest deviations to the unforced result are less than 0.5 mOD.

Associating these time constants with dynamic and kinetic processes is usually done in a two-temperature model for electronic thermalization (≈ tens of femtoseconds) and electron-phonon scattering (≥ hundreds of femtoseconds), followed by carrier recombination (in oxides ≥ picoseconds), and thermalization (≥ tens picoseconds), albeit trapped states and lateral thermal relaxation may also contribute to long-lived absorbance changes.

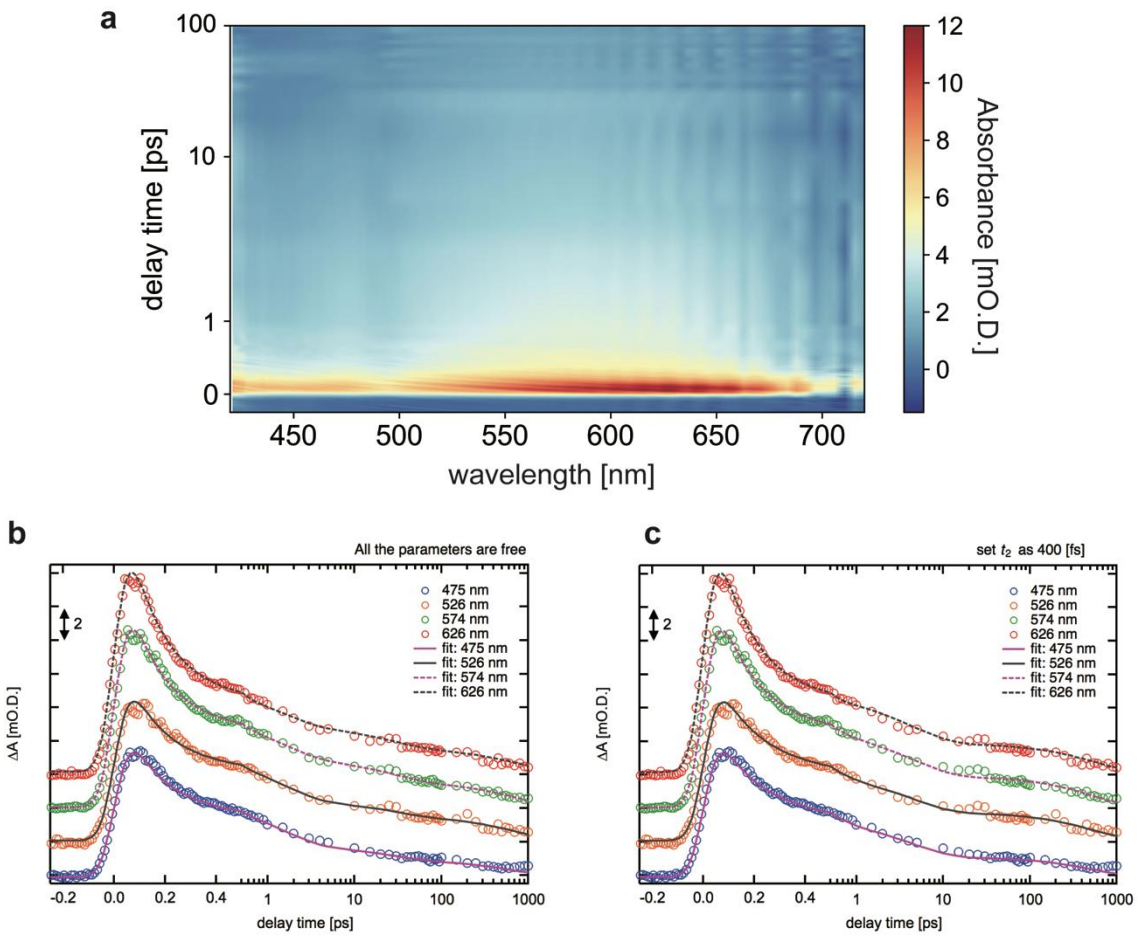

Figure S2. Optical pump probe spectroscopy of $CuWO_4$: (a) the transient response of $CuWO_4$ in the UV-Vis spectral region up to a delay time of 100 ps, (b) and (c) the kinetic traces at probes wavelengths of 475 nm, 526 nm, 574 nm, and 626 nm. All the kinetic constants used in fitting were free (no constraint) in (b) whereas a kinetic constant denoted as t_2 was fixed to 400 fs in (c).

3) Time-resolved X-ray Absorption Spectroscopy at PAL-XFEL

Experimental setup

All Cu L_3 XAS spectra were measured in the soft X-ray spectroscopy and scattering (SSS) beamline of PAL-XFEL. [4, 5] An overview of the SSS beamline instrument of PAL-XFEL is shown in Figure S3. In the SSS beamline, soft X-rays between 250 eV and 1200 eV are available. In order to monochromatize the X-ray, a grating optics with 200 lines per mm was employed. The estimated energy resolution of the X-ray for our experiments was ~ 0.5 eV at 930 eV. The monochromatized X-ray was focused by a pair of Kirkpatrick-Baez mirrors to reduce the X-ray size to less than 50 μm (*H*) × 50 μm (*V*) on the sample position. A spectrometer for emitted X-ray is equipped to the sample chamber in order to measure resonant inelastic X-ray scattering (RIXS). The X-ray dispersed by the monochromator is introduced to a CCD detector.

Since the X-ray intensity usually changes significantly for each X-ray pulse in XFELs, it is necessary to measure the monochromatized X-ray intensity (I_0) and the fluorescent X-ray intensity (I_f) shot by shot in order to obtain XAS correctly. In our experiments, each I_0 intensity was measured by counting the electrons emitted from a Si_3N_4 thin-film by using a microchannel plate (MCP) detector. The I_f intensity was measured with another MPC detector by obtaining fluorescent X-ray photons emitted from the sample. Two boxcar integrators (SR250, Stanford Research Systems) were employed to collect both the signals (I_0, I_f) from the MCP detectors. The data accumulation of the boxcars was synchronized with the trigger signals from the XFEL in order to gather only the signals from the X-ray pulses. The output signals from the boxcars were transferred to the digitizers (SR245, Stanford Research Systems).

A Ti:sapphire laser was employed to excite the sample. Its fundamental wavelength (800 nm) was converted to 400 nm with a BBO crystal. The laser pulses were transferred into the measurement chamber and focused on the sample position. The spot size of the laser was approximately 210 μm (*H*) × 210 μm (*V*) for its $1/e^2$ value. The angle between the X-ray and the laser was less than 1°. The excitation laser fluence was set to ~50 mJ cm^{-1}, which was found to be the optimum laser fluence and in the same time causing minimal to no sample damage or nonlinear effects. The repetition rate of the excitation laser was set to exactly the same rate as the XFEL using radio frequency signals. Since the excitation laser was synchronised with the XFEL[4], the jitter between the excitation laser and the XFEL was small and the estimated time resolution was less than 100 fs. In order to observe the evolution of photoexcited states of Cu^{2+} in $CuWO_4$, Cu L_3 XAS spectra were measured at different delay times by changing the timing between the XFEL pulses and the excitation laser pulses.

The X-ray intensity fluctuates shot-by-shot and the low-intensity shots were removed from the measurements as they create a low signal to noise ratio. A reference XAS spectrum at a delay time of -10 ps, i.e. an excitation laser pulse arrives at the sample 10 ps after an X-ray pulse arrives, was measured for

each measurement in order to calculate a difference spectrum for each delay time. We note that time instabilities in the intensity of XFEL pulses were observed over several hours. Such instability could affect the XAS signal and result in artificial differential spectra. To avoid these artifacts, the XAS at each delay time and those at the reference were measured in sequence.

Analysis of X-ray absorption data in PAL-XFEL

Since the intensity of each X-ray pulse fluctuates a lot in XFELs, the data acquisition system in XFELs should have a wide dynamic range. However, some of X-ray pulses have too low or large intensity to measure precisely. It is important to eliminate such X-ray pulses in order to obtain a XAS spectrum with a good signal-to-noise ratio (S/N). In our experiment in PAL-XFEL, the I_0 and I_f were recorded from 0 to 10 V. We set the lower and upper thresholds for I_0 and I_f. After analysing the XAS data sets, we found that if X-ray shots whose I_0 or I_f value was > 2.0 V or < 8.0 V were included, the S/N of a XAS spectrum got significantly worse. Therefore, we used the X-ray pluses whose I_0 and I_f values were between 2.0 V and 8.0 V. In addition to the thresholds, the average (avg_{XAS}) and the standard deviation (σ_{XAS}) of I_f/I_0 i.e. XAS for each X-ray pulse was used. If the absolute value of I_f/I_0 - avg_{XAS} for an X-ray pulse was less than σ_{XAS}, the X-ray pulse was included for the calculation of XAS. According to these thresholds, we accumulated typically ~550 shots for each energy or delay point. The ratio of the transient signals to the statistical error was estimated as more than 10.

For differential XAS spectra, we estimated uncertainties based on the difference XAS at a delay of -5 ps since the statistical uncertainties are smaller than the standard deviation of the difference XAS at a delay of -5 ps. The statistical uncertainties of the difference XAS at -5 ps below 0.004 for each XAS data point as shown in Figure 2. On the other hand, the standard deviation of the difference XAS at a delay of -5 ps is 0.0067. If only statistical errors were crucial for the uncertainties, this value would be below 0.004. There are other factors which contributed to the uncertainties of our data sets. In order to avoid underestimating the uncertainties, we estimated the uncertainties from the difference XAS at a delay of -5 ps. It should be noted that statistical errors in difference XAS at other delays are similar to the statistical uncertainties of the difference XAS at -5 ps. For the kinetic traces, the uncertainties were estimated based on the reference kinetic trace i.e. a delay time of -5 ps as the same reason of the differential XAS spectra.

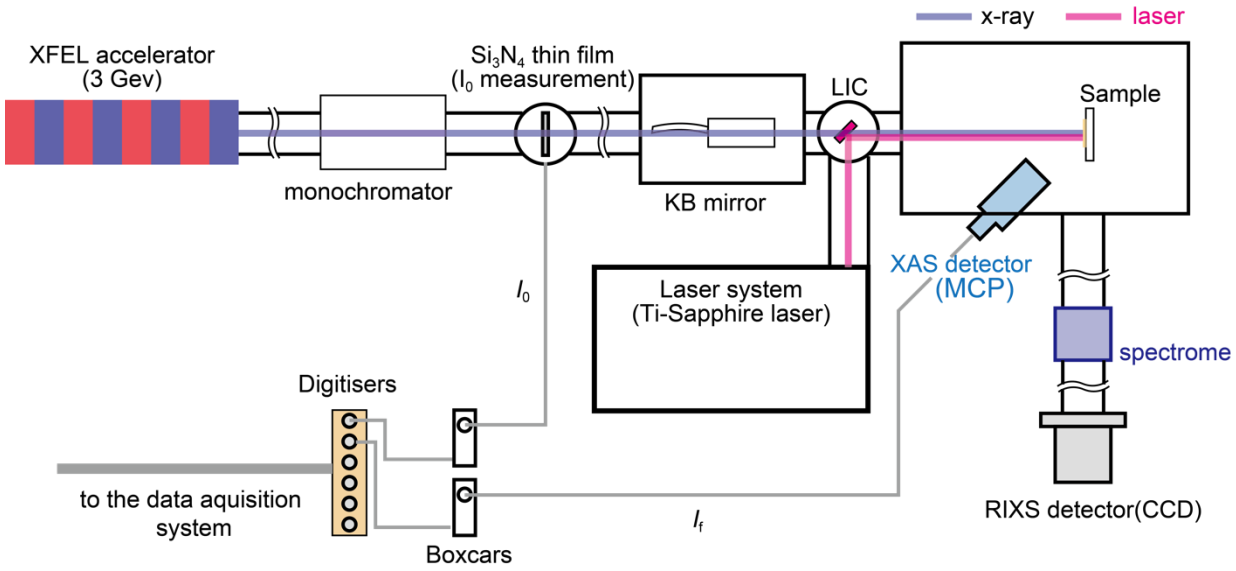

Figure S3. The experimental setup of the SSS beamline of PAL-XFEL. A microchannel plate (MCP) detector was employed to measure the fluorescent X-ray intensity.

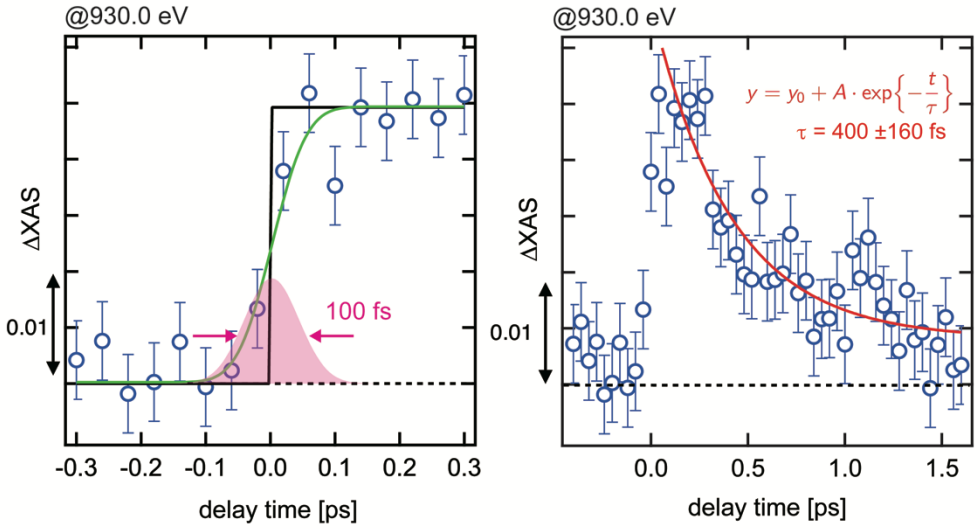

Figure S4. The kinetic trace of X-ray absorption spectroscopy (XAS) at 930.0 eV: (I) the estimation of the time resolution of the setup, as shown in Figure S3. (II) the estimation of the kinetic constant of the fast decay process.

4) The experimental setup at BL07LSU, SPring-8

Transient XAS spectra of the Cu L_3 edge in hundreds of picoseconds were obtained at the BL07LSU beamline in SPring-8. During the beamtime, the operation mode of SPring-8 was ''H-mode'', [6] where one isolated electron bunch is found between electron bunch trains. The isolated electron bunch produces an X-ray pulse whose pulse duration is ~80 ps and the X-ray pulse arrives at the beamtime every ~4.76 μs (~210 kHz). In order to synchronize with the excitation laser (~1 kHz), an X-ray chopper developed in SPring-8 [7] was employed to the repetition rate of the X-ray pulse. XAS spectra were measured by collecting Auger electrons emitted from the sample surface (Partial Electron Yield (PEY)). An MCP detector was employed to measure the intensity of electrons from the sample surface. The fluence of the excitation laser was the same as in PAL-XFEL and the temporal resolution of the set up was estimated to be 80 ps. Further details on the setup were explained in ref. 8. The excitation laser wavelength was 400 nm and the fluence was ~ 20 mJ/cm^2.

5) Time resolved X-ray Absorption Spectroscopy in SACLA

Experimental setup

Pump probe experiments of the Cu K-edge XAS were carried out at the EH2 in SPring-8 Angstrom Compact Free Electron Laser (SACLA) [9, 10]. A pair of Si(111) channel-cut crystals were employed to monochromatize the X-ray pulses, which were focused with Be lenses, and the focal size of X-ray was less than 5 μm(H) x 5 μm(V). [11, 12] XAS was measured in a fluorescence geometry. The intensity of the elastically scattered X-ray pulses was measured using two photodiodes to measure the incident X-ray intensity, while the fluorescence X-rays emitted from the sample were measured using a Multi-Port CCD (MPCCD) [13] detector developed in SACLA. An X-ray fluorescence filter was placed in front of the MPCCD detector in order to attenuate elastic scattering X-ray photons. Since each element on the MPCCD detector has an energy resolution of ~1 keV for X-ray photons, the Cu Kα X-ray photons were accumulated selectively in data processing process. The intensity of Cu Kα X-ray fluorescence was estimated by the number of X-ray photons detected in the MPCCD (photon counting mode). A chirped-pulse amplified laser was used in order to excite the sample. The pulse duration was approximately 50 fs, a wavelength of 400 nm, and a fluence of ~ 60 mJ cm^2. A $CuWO_4$ thin film sample with a thickness of 50 nm was employed, whose sample characteristics were the same as the sample we have measured in PAL-XFEL.

Analysis of X-ray absorption data in SACLA

In order to analyze the data measured in SACLA, we used a similar procedure of data analysis conducted in PAL-XFEL. Since the intensity of each X-ray pulse fluctuate a lot, X-ray shots whose incident X-ray intensity (I_0) was too small or too large to measure were eliminated. Then, the intensity of X-ray

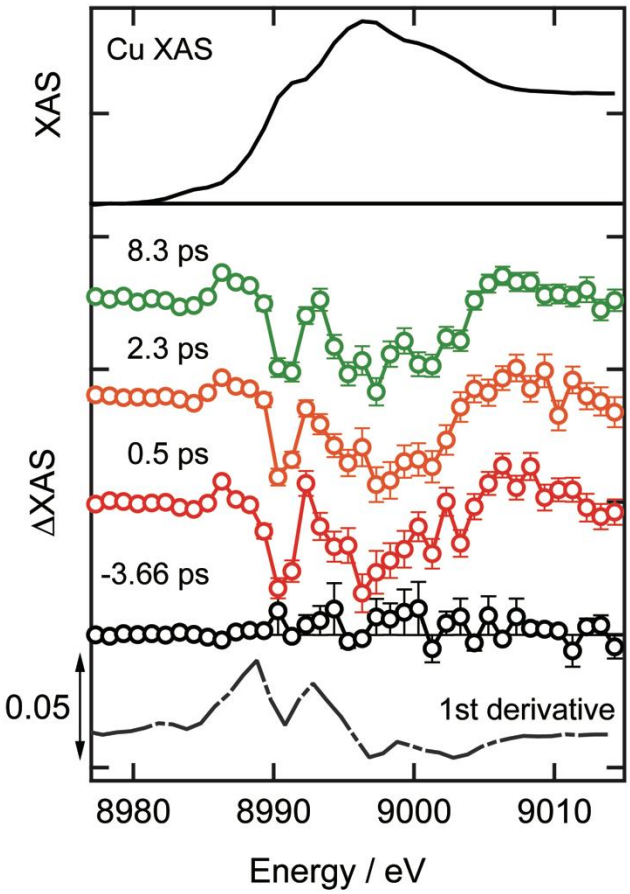

Figure S5. Pump probe Cu K-edge X-ray absorption spectroscopy (XAS) measured in SACLA: transient XAS at a delay time of -3.66 ps, 0.5 ps, 2.3 ps and 8.3 ps. '1st derivative' is a first derivative of a static Cu K-edge XAS spectrum shown in the top panel.

fluorescence (I_f) was plotted against I_0 for each energy point. The intensity of X-ray fluorescence was the photon count measured by MPCCD whereas I_0 was the output voltage from the photodiodes (0 to 1 V). If the I_0 value was between 0.001 V and 0.1 V, I_f was linear to I_0. However, I_0 became greater than 0.1 V, the linearity broke down and I_f was smaller than expected. This is because the number of X-ray photons coming into MPCCD was beyond its counting ability. Therefore, the linearity between I_f and I_0 got worse as I_0 became larger. Eventually, we employed the threshold for I_0 to pick up X-ray pulses whose I_f was linear to I_0. Normally, 300 – 500 shots were taken based on the threshold. After the data selection, XAS was calculated for each X-ray shot and average the calculated XAS values for each energy point. The uncertainty of XAS for each energy point was evaluated based on a standard error of the XAS data sets i.e. the standard deviation of the XAS data sets divided by the square root of the number of X-ray shot taken according to the threshold. The ratio of the uncertainty to the transient signal was between 0.1 and 0.3 depending on

energy point. As shown in Figure S5, transient XAS signals are significantly larger than the uncertainties. It should be noted that the standard deviation of difference XAS at -3.66 ps is as small as the uncertainties of it. This implies that the statistical uncertainties are dominant in the uncertainties in the XAS data sets measured in SACLA. Therefore, we employed the statistical uncertainties as the uncertainties for the XAS data sets.

In Figure S5, transient Cu K-edge XAS are displayed. There were two regions observed where transient signals appeared. One region is around 8890 eV. The XAS at this energy decreased after photoexcitation by the laser. The other region is around 9000 eV. The transient feature in this region is a broad beaching peak. Comparing to the 1st derivative of a static Cu K-edge XAS of the $CuWO_4$ thin film, these features are supposed to come from the overall spectrum shift to lower energy. This is because the charge density at the Cu sites were enhanced after the photoexcitation to decrease the threshold energy of the X-ray absorption, which is consistent to what we observed in PAL-XFEL.

In order to explore the dynamics after the photoexcitation, the kinetic trace at 8990 eV was measured. The time resolution of the transient XAS experiments at SACLA was ~ 500 fs owing to a time jitter. In order to observe the dynamics in the very early stage of the photoexcitation (< 1 ps), we employed the arrival timing monitor (ATM) developed in SACLA. [14] ATM can estimate the actual timing jitter between an X-ray pulse and a laser pulse. Its precision is ~ 7 fs. In order to correct the delay time, the XAS signal for each X-ray shot was sorted according to the observed jitter value of the ATM. Then, the XAS signals were averaged according to the defined delay steps. For these experiments, we set a delay step of 96.3 fs. As the result of the timing analyses, a fast decay kinetic process was found (Figure 3 (d)).

1. Yourey, J. E.; Bartlett, B. M., Electrochemical deposition and photoelectrochemistry of $CuWO_4$, a promising photoanode for water oxidation. *J. Mater. Chem.* **2011**, *21*, 7651-7660.

2. Pesci, F. M.; Cowan, A. J.; Alexander, B. D.; Durrant, J. R.; Klug, D. R., Charge Carrier Dynamics on Mesoporous WO_3 during Water Splitting. *J. Phys. Chem. Lett.* **2011**, *2*, 1900-1903.

3. Sachs, M., et al., Effect of oxygen deficiency on the excited state kinetics of WO_3 and implications for photocatalysis. *Chem. Sci.* **2019**, *10*, 5667-5677.

4. Kang, H.-S., et al., Hard X-ray free-electron laser with femtosecond-scale timing jitter. *Nat. Photonics* **2017**, *11*, 708-713.

5. Park, S. H., et al., PAL-XFEL soft X-ray scientific instruments and X-ray optics: First commissioning results. *Rev. Sci. Instrum.* **2018**, *89*, 055105.

6. Valenti, M.; Dolat, D.; Biskos, G.; Schmidt-Ott, A.; Smith, W. A., Enhancement of the Photoelectrochemical Performance of $CuWO_4$ Thin Films for Solar Water Splitting by Plasmonic Nanoparticle Functionalization. *J. Phys. Chem. C* **2015**, *119*, 2096-2104.

7. Osawa, H.; Ohkochi, T.; Fujisawa, M.; Kimura, S.; Kinoshita, T., Development of optical choppers for time-resolved measurements at soft X-ray synchrotron radiation beamlines. *J. Synchrotron Radiat.* **2017**, *24*, 560-565.

8. Takubo, K., et al., Capturing ultrafast magnetic dynamics by time-resolved soft X-ray magnetic circular dichroism. *Appl. Phys. Lett.* **2017**, *110*, 162401.

9. Ishikawa, T., et al., A compact X-ray free-electron laser emitting in the sub-ångström region. *Nat. Photonics* **2012**, *6*, 540-544.

10. Tono, K., et al., Beamline, experimental stations and photon beam diagnostics for the hard X-ray free electron laser of SACLA. *New J. Phys.* **2013**, *15*, 083035.

11. Katayama, T.; Nozawa, S.; Umena, Y.; Lee, S.; Togashi, T.; Owada, S.; Yabashi, M., A versatile experimental system for tracking ultrafast chemical reactions with X-ray free-electron lasers. *Struct. Dyn.* **2019**, *6*, 054302.

12. Katayama, T.; Hirano, T.; Morioka, Y.; Sano, Y.; Osaka, T.; Owada, S.; Togashi, T.; Yabashi, M., X-ray optics for advanced ultrafast pump-probe X-ray experiments at SACLAThis article will form part of a virtual special issue on X-ray free-electron lasers. *J. Synchrotron Radiat.* **2019**, *26*, 333-338.

13. Kameshima, T., et al., Development of an X-ray pixel detector with multi-port charge-coupled device for X-ray free-electron laser experiments. *Rev. Sci. Instrum.* **2014**, *85*, 033110.

14. Katayama, T., et al., A beam branching method for timing and spectral characterization of hard X-ray free-electron lasers. *Struct. Dyn.* **2016**, *3*, 034301.